nature structural biology



# Sequence elements outside the hammerhead ribozyme catalytic core enable intracellular activity

Anastasia Khvorova[1,2], Aurélie Lescoute[3], Eric Westhof[3] & Sumedha D Jayasena[1]

**The hammerhead ribozyme (HHRz) is a small, naturally occurring ribozyme that site-specifically cleaves RNA and has long been considered a potentially useful tool for gene silencing. The minimal conserved HHRz motif derived from natural sequences consists of three helices that intersect at a highly conserved catalytic core of 11 nucleotides. The presence of this motif is sufficient to support cleavage at high $Mg^{2+}$ concentrations, but not at the low $Mg^{2+}$ concentrations characteristic of intracellular environments. Here we demonstrate that natural HHRzs require the presence of additional nonconserved sequence elements outside of the conserved catalytic core to enable intracellular activity. These elements may stabilize the HHRz in a catalytically active conformation via tertiary interactions. HHRzs stabilized by these interactions cleave efficiently at physiological $Mg^{2+}$ concentrations and are functional *in vivo*. The proposed role of these tertiary interacting motifs is supported by mutational, functional, structural and molecular modeling analysis of natural HHRzs.**

Previous analysis of numerous mutant HHRz variants[1] has indicated that the length and sequence composition of the three stem-loops are not important for *in vitro* catalysis, provided that the conserved catalytic core and the three-way junction are preserved. The catalytic activity of such minimalist HHRzs is strongly dependent on $Mg^{2+}$ ions, with the optimal cation concentration exceeding 10 mM. At physiological $Mg^{2+}$ concentrations (0.1–0.3 mM)[2], these minimalist HHRzs are almost inactive, whereas natural HHRzs are apparently functional. The objective of this study was to determine which sequence or structural features, if any, enable natural HHRzs to be functional at low $Mg^{2+}$ concentrations.

## RESULTS

### Catalytic activity of natural vs. minimalist HHRzs

The intracellular activity of various *cis*-cleaving HHRzs was evaluated using a reporter gene expression assay[3] (**Fig. 1a**). *Cis*-cleaving HHRzs were cloned into a unique site within the 3′-untranslated region (3′ UTR) of bovine growth hormone (BGH) directly downstream of the reporter gene, secreted alkaline phosphatase (SEAP). The presence of an active *cis*-cleaving HHRz in the 3′ UTR leads to the cleavage of the SEAP mRNA, resulting in the loss of protein expression. When HHRz from satellite RNA of tobacco ringspot virus (sTRSV)[4] was inserted, expression of SEAP was reduced (**Fig. 1b**). By contrast, insertion of HHR15 (one of the minimalist HHRzs that cleaves to completion *in vitro* with a $k_{cat}$ of 1 $min^{-1}$ at 10 mM $Mg^{2+}$) or a double mutant of the sTRSV ribozyme (G5-C5; C17-G17) had no effect on SEAP expression. In each case, SEAP mRNA levels (**Fig. 1b**, gray bars) closely matched SEAP protein levels (**Fig. 1b**, black bars), indicating that ribozyme activity suppressed reporter gene expression.

The intracellular performance of sTRSV and HH15 is representative of two ribozyme classes: all natural ribozymes tested reduced SEAP expression efficiently, whereas none of the more than 20 minimalist HHRzs tested were active (data not shown). *In vitro* cleavage kinetics of HHRzs from sTRSV, lucerne transient streak virus (vLTSV) and peach latent mosaic viroid (PMLVD)[4–6], as well as one of the standard minimalist HHRzs, HH2 (ref. 7), were compared under conditions approximating intracellular $Mg^{2+}$ concentrations (0.1 mM). All three natural HHRzs demonstrated efficient cleavage at 0.1 mM $MgCl_2$, with initial rates ($k_{obs}$) varying from 0.7 $min^{-1}$ to 1.4 $min^{-1}$ (**Fig. 1c** and **Table 1**). By contrast, the minimalist *cis*-cleaving HH2 exhibited very low activity, with an initial rate of 0.02 $min^{-1}$.

The rate of cleavage ($k_{obs}$) of the two types of HHRzs was then determined as a function of $Mg^{2+}$ concentration (**Fig. 1d** and **Table 1**) (at a $Mg^{2+}$ concentration >200 μM, the cleavage rates of natural HHRzs were >2.5 $min^{-1}$, too fast to measure manually). The $k_{obs}$ of natural HHRzs reached the benchmark value of 1 $min^{-1}$ at ~0.07 mM $Mg^{2+}$ (defined as $[Mg^{2+}]_{eff}$), whereas the $[Mg^{2+}]_{eff}$ of HH2 was >10 mM[8]. The catalytic efficiency of natural HHRzs at submillimolar concentrations of $Mg^{2+}$ correlates well with their vigorous intracellular activity, whereas the poor *in vitro* cleavage of minimalist HHRzs at 0.1 mM $Mg^{2+}$ is consistent with their lack of intracellular activity.

### Structural difference between natural and minimalist HHRzs

Both natural and minimalist ribozymes contain the catalytic core of 11 conserved nucleotides, and both cleaved to completion in the *in vitro* assay at 10 mM $Mg^{2+}$. The major structural difference between the two

[1]Amgen, Inc., One Amgen Center Drive, Thousand Oaks, California 91320, USA. [2]Present address: Dharmacon Research, Inc., 1376 Miners Drive, #101, Lafayette, Colorado 80026, USA. [3]Institut de Biologie Moléculaire et Cellulaire, UPR9002 du CNRS, Université Louis Pasteur, 15 rue René Descartes F-67084, Strasbourg Cedex, France. Correspondence should be addressed to A.K. (khvorova.a@dharmacon.com) or S.D.J. (sumedhaj@amgen.com).

Published online 27 July 2003; doi:10.1038/nsb959

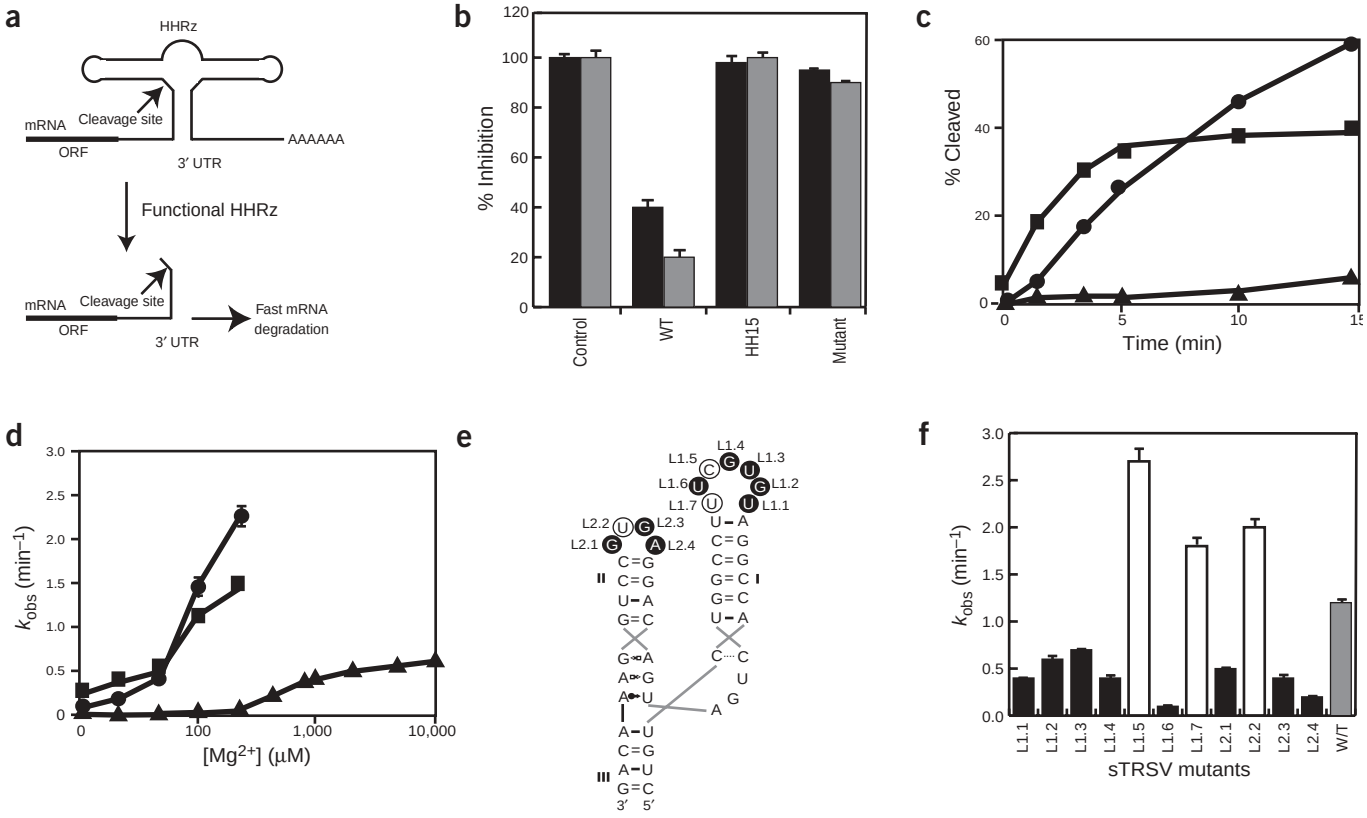


**Figure 1** *In vitro, in vivo*, and mutational analysis of natural HHRzs. (**a**) Schematic representation of the reporter gene expression assay used to evaluate intracellular *in vivo* function of HHRzs in tissue culture[3]. (**b**) Transient gene expression assay conducted using plasmids carrying no HHRz (control), sTRSV (WT, wild type), HH15 (minimalist HHRz) or mutant HHRz within the 3′ UTR of the SEAP gene. SEAP protein (black bars) and mRNA (gray bars) levels produced by each plasmid were normalized to the control. (**c**) *In vitro* cleavage kinetics of sTRSV (circles), PMLVD (squares) and minimalist HH2 (triangles) at various time points in 0.1 mM $Mg^{2+}$ at pH 7.0. (**d**) $Mg^{2+}$ dependence of HHRz activity. Observed rate of cleavage ($k_{obs}$) is plotted as a function of [$Mg^{2+}$] for sTRSV (circles), PMLVD (squares) and HH2 (triangles). Error bars indicate standard deviation from the average of three independent measurements. (**e**) Schematic representation of sTRSV HHRz showing the 11 unpaired nucleotides in loops I and II that were subjected to point mutation. Nomenclature follows ref. 30. (**f**) $k_{obs}$ values measured at 0.1 mM $Mg^{2+}$ for each point mutant, showing the increase (open bars) or decrease (solid bars) in catalytic activity relative to wild-type sTRSV HHRz (gray bar) performance.

types is that minimalist HHRzs lack the loops capping helices I and II. To test the influence of the nucleotide composition of loops I and II on HHRz activity at low $Mg^{2+}$ concentrations, a set of sTRSV HHRz point mutants was generated by systematic substitution of each of the 11 unpaired nucleotides in loops I and II with cytosine (C5 was substituted with guanosine; **Fig. 1e**). Mutations at 8 of the 11 positions yielded a reduced cleavage rate ($k_{obs}$) (**Fig. 1f**), whereas substitution at positions 5, 7 and 9 increased the cleavage rate as compared with that of the wild-type ribozyme (**Fig. 1f**, open bars). This mutational analysis demonstrates that the specific nucleotide sequence of loops I and II of sTRSV is critical for enabling catalysis.

**Table 1 Kinetic parameters of HHRz cleavage reactions**

| Ribozyme | $k_{obs}$ (min$^{-1}$) | Change in activity (fold) | [$Mg^{2+}$]$_{eff}$ (mM) |
|---|---|---|---|
| STRSV | 1.20 | 1 | 0.07 |
| VLTSV | 1.40 | 0.90 | ND |
| STRSV+LT-1 | 0.16 | 7.50 | ND |
| STRSV+LT-2 | 0.05 | 26.7 | ND |
| STRSV+LT-1&2 | 1 | 1.20 | ND |
| PMLVD | 0.71 | 1.70 | 0.06 |
| STRSV+PL-1 | 0.11 | 10.90 | 0.93 |
| STRSV+PL-2 | <0.01 | >100 | >5.0 |
| STRSV+PL-1&2 | 0.41 | 2.90 | 0.04 |
| HH2 | 0.02 | 50 | >10.0 |

Measurements were made at 37 °C in 50 mM Tris-HCl, pH 7.0, and 0.1 mM $MgCl_2$. Change in activity calculated by $k_{obs}$ of chimeric HHRz divided by $k_{obs}$ of sTRSV. In each case, the [$Mg^{2+}$]$_{eff}$ represents the concentration of $MgCl_2$ required to produce a $k_{obs}$ value of 1 min$^{-1}$. ND, not determined.

## Modeling of loop I–loop II interactions

The proximity of helices I and II within the structure of HHRzs[9,10] suggests possible loop I–loop II interactions. The majority of HHRzs are embodied within the viral RNA sequence through stem III. The sequence alignments of helix III–integrated HHRzs (**Fig. 2**) show that loops I and II are usually comprised of three or four nucleotides, exhibiting significant similarity with loops 6 and 8 of the signal recognition particle (SRP) domain[11,12]. Models of the interactions between the two loops were built using crystal structures of hammerhead ribozymes[9,10] and the library of RNA structures[13]. Loop-loop interactions analogous to those of SRP three-dimensional structures were built for sTRSV HHRz (**Fig. 3**) using the MANIP program[14]. Interloop interactions arise from a *trans* Watson-Crick–Watson-Crick pair between the third residue of LII (L2.3 in **Fig. 1e**) and the last residue of

LI (L1.5 in **Fig. 1e**) together with a *trans* sugar-sugar pair between the last residue of LII (L2.4 in **Fig. 1e**) and the 3′-end residue (L1.7) of the loop 1 capping helix I. The enhanced cleavage of point mutants in positions L1.5, L1.7 and L2.2 can be explained by a formation of alternative base pairs that can be easily modeled: the L1.5 mutant leads to a *trans* Watson-Crick–Watson-Crick pair, the L1.7 mutant to a *cis* Watson-Crick–Watson-Crick pair as in sLTSV, and we suggest that the mutant L2.2 leads to the formation of an additional Watson-Crick C-G pair. In 12 natural HHRzs (**Fig. 2**), we found five A-U pairs, one G-C pair and one U-A pair with the potential to act as the *trans* Watson-Crick–Watson-Crick pair. Depending on the number of base pairs in helices I and II, the sequence and length of loops I and II vary in order to maintain loop-loop interactions. The models for vLTSV and PMLVD HHRzs were built using the same architectural rules as for sTRSV (**Fig. 4a**). In all models, the structure of the ribozyme core was not altered below the first Watson-Crick pair of helices I and II (**Fig. 3**). Similar to sTRSV, PMLVD and vLTSV also showed interloop interactions through *trans* Watson-Crick–Watson-Crick and *trans* sugar-sugar interactions. This observation is consistent with the catalytic activity of these HHRzs at 0.1 mM $Mg^{2+}$.

| | CS | Stem I | LI | Stem I′ | Core | Stem | LII | Stem II′ | Core | Stem III′ |
|---|---|---|---|---|---|---|---|---|---|---|
| **vVTMoV+** | UCCG | UA GUGGAU | GUG**U** | AUCCACU | CUGAUGA | GUCC | GA**A**A | GGAC | GAAA | CGGA |
| **sBYDV–** | GGUG | UC UCAAGGU | GCG**U** | ACCUUGA | CUGAUGA | GUCC | GA**A**A | GGAC | GAAA | CACC |
| **Scc+** | AUGCUG | UA GUGGGAU | GUG**U** | GUCUCAC | CUGAAGA | GUAC | A**A**AA | GUCC | GAAA | CGGUAU |
| **Scc–** | GCUA | UA UGGGGAU | GUG**U** | GUCCCUA | CUGACGA | GUUC | A**A**AA | GAAC | GAAA | UAGU |
| **vSCMoV+** | CGCUG | UC UGUACUU | GUA**U** | CAGUACA | CUGACGA | GUCCC | U**A**AA | GGAC | GAAA | CACCG |
| **sTRSV+** | CCUG | UC ACCGGAU | GUG**C** | UUUCCGGU | CUGAUGA | GUCC | GU**G**A | GGAC | GAAA | CAGG |
| **SarMV+** | ACUG | UC GCCGGAU | GU**G**U | AUCCGAC | CUGACGA | UGGCCC | A**A**AA | GGGCC | GAAA | CAGU |
| **sLTSV+** | UACG | UC UGAGCGU | GA**U**A | CCCGCUCA | CUGAAGA | UGGCCC | GG**U**A | GGGCC | GAAA | CGUA |
| **CChMVd+** | AAGAGG | UC GGCACCU | GAC**G** | UCGGUGUC | CUGAUGA | AGAUCCAU | GA**C**A | GGAUC | GAAA | CCUCUU |
| **sLTSV–** | GACGUA | UGAGACU | GACUGAAA | CGCCGUCUCA | CUGAUGA | GGCCAU | GG**C**A | GGCC | GAAA | CGUC |
| **SCYMV+** | UACUG | UC GCCAGAC | GUG**G** | ACCCGGC | CUGAUGA | GUCC | GA**A**A | GGAC | GAAA | CAGUA |
| **PLMVd–** | UCAUAAG | UC | UGGGC | U**A**A | GCCCA | CUGAUGA | GUCGCU | GAAA | UGCGAC | GAAA CUUAUGA |
| **PLMVd+** | GAAGAG | UC | UGUGC | U**A**A | GCACA | CUGACGA | GUCUCU | GAGA | UGAGAC | GAAA CUCUUC |

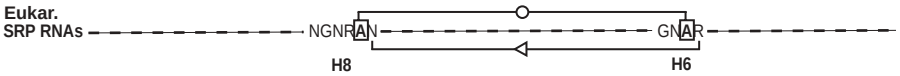


**Figure 2** Sequence alignment of natural HHRzs integrated through stem III. HHrzs are named by origin: vVTMoV, velvet tobacco mottle virusoid; sBYDV, barley yellow dwarf virus satellite RNA; Scc, small circular cherry RNA; vSCMoV, subterraneum clover mottle virusoid; sTRSV, tobacco ringspot virus satellite RNA; sLTSV, lucerne transient streak virusoid; CChMVd, chrysanthemum chlorotic mottle viroids; sCYMV, chicory yellow mottle virus satellite RNA; PMLVd, peach latent mosaic viroid. Structurally modeled ribozymes (**Figs. 3** and **4**) are indicated in red. CS, cleavage site; core, invariant catalytic core. The residues interacting between loops 1 and 2 are in bold. Consensus sequences (archaea and some eukaryotes) for loop sequences[31] (loops L6 and L8 capping helices 6 and 8) are shown at the bottom with interacting residues in bold and symbols (circle, *trans* Watson-Crick–Watson-Crick; triangle, *trans* sugar-sugar) for types of base pairs.

To verify the existence of the interloop contacts, a set of chimeric HHRzs based on sTRSV, vLTSV and PMLVD was synthesized. Chimeras were generated by swapping loop I, loop II or both loop I and loop II of sTRSV with the corresponding loops from either vLTSV or PMLVD (**Fig. 4b**; only one set of swaps between sTRSV and PMLVD is shown). A loop I or II substitution either weakened (in the case of sTRSV+PL-1) or completely eliminated (in the case of sTRSV+PL-2) interloop interaction in these chimeras. The interloop interactions in the chimeric molecule with both loops substituted (sTRSV+PL1&2) were similar to those of the PMLVD ribozyme. Kinetically, replacement of loops I or II of the sTRSV by the corresponding loops of vLTSV and PMLVD resulted in a 7- to >100-fold loss of activity (**Fig. 4c** and **Table 1**) and a 10- to 100-fold increase in $[Mg^{2+}]_{eff}$ (**Fig. 4d** and **Table 1**). The simultaneous replacement of both loops of sTRSV with loop I and loop II sequences from either vLTSV or PMLVD restored the rate of cleavage and $[Mg^{2+}]_{eff}$ to near wild-type levels (**Figs. 4a,b** and **Table 1**). This finding indicates that the nucleotide sequences of loops I and II derived from PMLVD and vLTSV retained their compatibility and formed tertiary interactions in the background of the sTRSV ribozyme (**Fig. 4b**).

Finally, the intracellular activity of chimeric HHRzs was tested using the reporter gene assay. All three natural HHRzs were

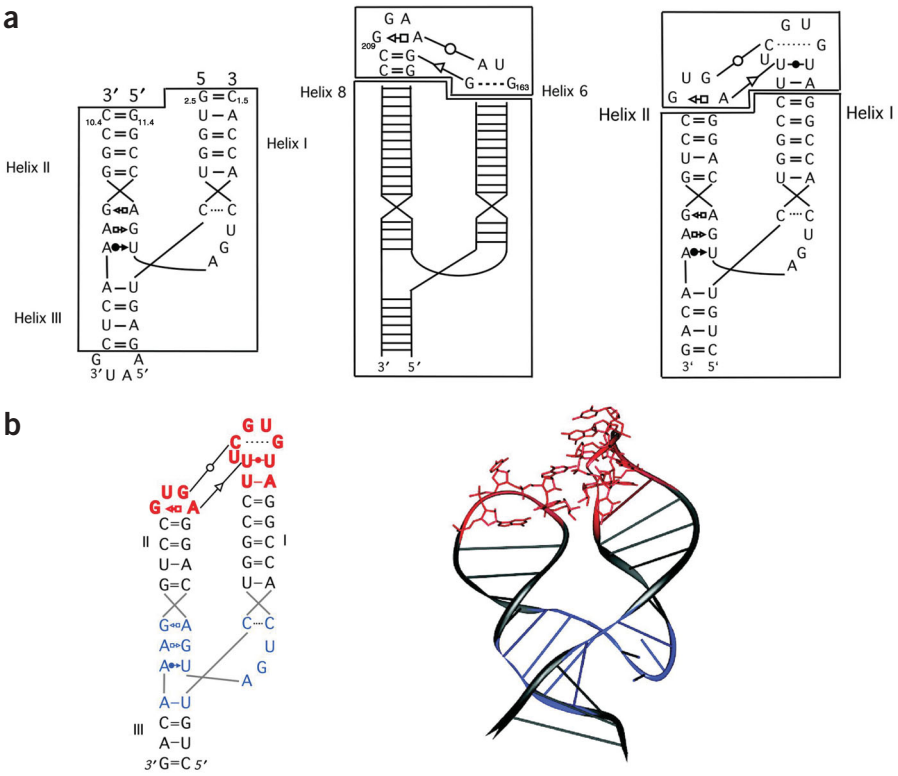


**Figure 3** Structural modeling of the sTRSV HHRz. (**a**) Secondary structures illustrating analogy between three-way junction in hammerhead ribozyme (left) and SRP RNA[11] (middle). Loop-loop interaction linking helices 6 and 8 in SRP particle could be similarly modeled in natural ribozyme (right) between helices I and II. (**b**) 2D (left) and 3D views of modeled natural sTRSV HHRz. In 2D view, non-Watson-Crick pairs are shown using nomenclature of Leontis and Westhof[32]. Colors correspond to same regions in both views, with catalytic core in blue.

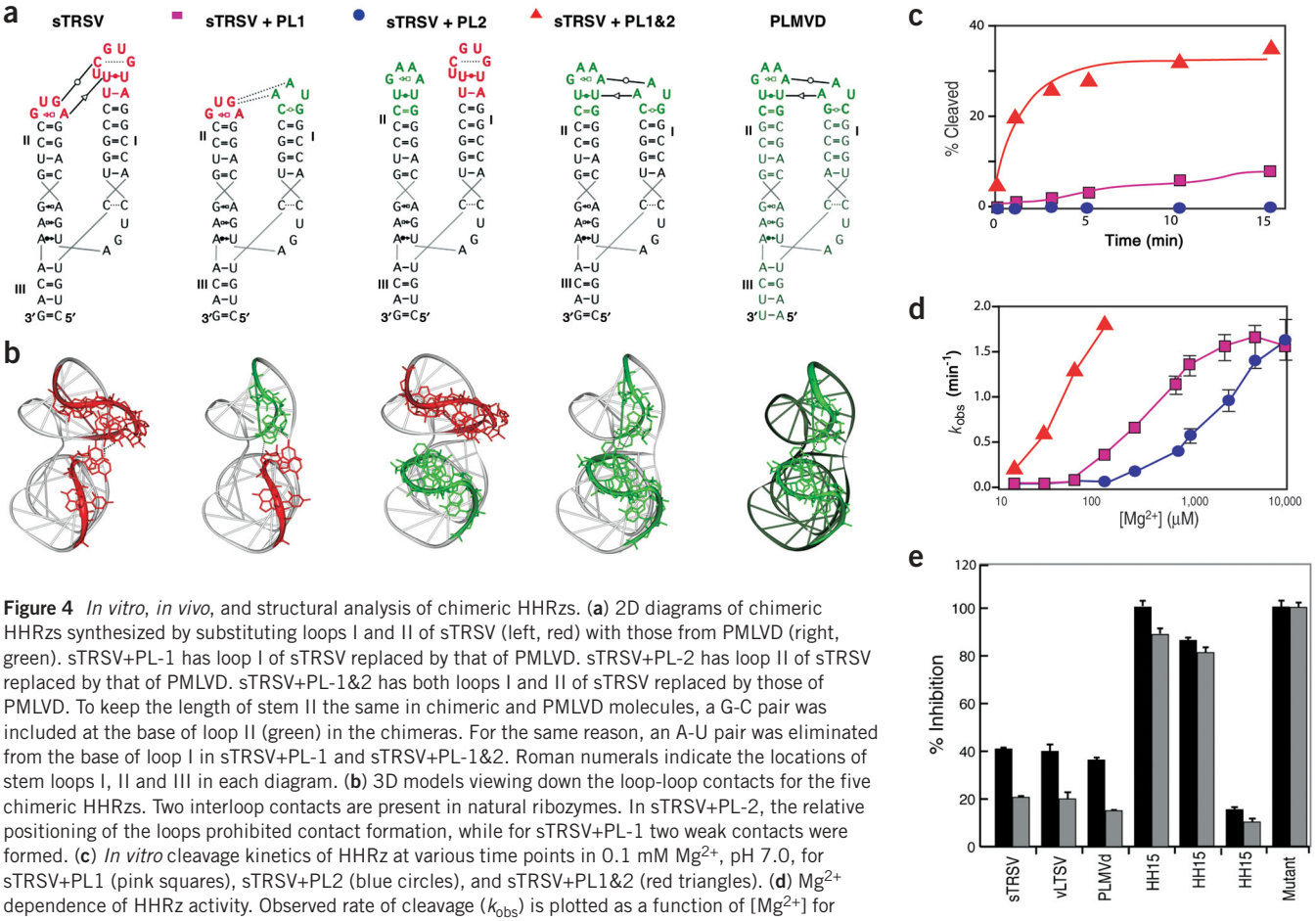


**Figure 4** *In vitro*, *in vivo*, and structural analysis of chimeric HHRzs. (**a**) 2D diagrams of chimeric HHRzs synthesized by substituting loops I and II of sTRSV (left, red) with those from PMLVD (right, green). sTRSV+PL-1 has loop I of sTRSV replaced by that of PMLVD. sTRSV+PL-2 has loop II of sTRSV replaced by that of PMLVD. sTRSV+PL-1&2 has both loops I and II of sTRSV replaced by those of PMLVD. To keep the length of stem II the same in chimeric and PMLVD molecules, a G-C pair was included at the base of loop II (green) in the chimeras. For the same reason, an A-U pair was eliminated from the base of loop I in sTRSV+PL-1 and sTRSV+PL-1&2. Roman numerals indicate the locations of stem loops I, II and III in each diagram. (**b**) 3D models viewing down the loop-loop contacts for the five chimeric HHRzs. Two interloop contacts are present in natural ribozymes. In sTRSV+PL-2, the relative positioning of the loops prohibited contact formation, while for sTRSV+PL-1 two weak contacts were formed. (**c**) *In vitro* cleavage kinetics of HHRz at various time points in 0.1 mM $Mg^{2+}$, pH 7.0, for sTRSV+PL1 (pink squares), sTRSV+PL2 (blue circles), and sTRSV+PL1&2 (red triangles). (**d**) $Mg^{2+}$ dependence of HHRz activity. Observed rate of cleavage ($k_{obs}$) is plotted as a function of [$Mg^{2+}$] for sTRSV+PL1 (pink squares), sTRSV+PL2 (blue circles), and sTRSV+PL1&2 (red triangles). Error bars indicate standard deviation from mean of three independent measurements. (**e**) HHRz catalytic activity in the *in vivo* reporter gene expression assay for the negative control (no HHRz), sTRSV, vLTSV, PMLVD, sTRSV+PL1, sTRSV+PL2 and sTRSV+PL1&2. Black and gray bars represent protein and mRNA levels, respectively.

active intracellularly, effectively reducing SEAP mRNA and protein levels as compared with those of the control (**Fig. 4e**). By contrast, chimeric ribozymes with only one loop of sTRSV swapped with a loop from PMLVD failed to cleave mRNA. When both loops of sTRSV were replaced with corresponding loops from PMLVD, the resulting chimeric HHRz was active *in vivo*. Similar intracellular results were seen with chimeric HHRzs derived from sTRSV and vLTSV (data not shown), indicating that the observed effect is a general phenomenon independent of the background of the ribozyme.

## DISCUSSION

### Loop I-loop II interactions and HHRz activity

Both intracellular and *in vitro* HHRz activity at low $Mg^{2+}$ concentrations correlate strongly with the ability of HHRz to form tertiary interactions between loops I and II, as demonstrated by mutational analysis and predicted by molecular modeling. All HHRzs—natural and chimeric—in which interactions between loops I and II could be modeled (**Fig. 4a**,**b**) cleaved efficiently at 0.1 mM $Mg^{2+}$ and were functional *in vivo*.

Although several crystal structures of the minimalist HHRzs are available[9,10], disagreement between structural and biochemical data exists[15]. The native loop-loop interaction proposed here incorporates the core structure, as derived from X-ray data (r.m.s. deviation between original X-ray structure and present models is ~0.8 Å; the majority of the discrepancy originates from the different refinement programs used). The tertiary interactions between loops I and II of natural HHRzs most likely restrict their relative movements, thereby helping to stabilize an HHRz conformational state that closely resembles the catalytically active conformation. Our finding that HHRzs stabilized by tertiary interactions exhibit a reduced requirement for $Mg^{2+}$ is consistent with the proposed biphasic HHRz folding model[16]. The second stage of the biphasic process involves folding of the catalytic domain in which stem I rotates to enable relatively close positioning to stem II; this stage requires an $Mg^{2+}$ concentration of ~10 mM. This finding is consistent with the activity profile of typical ribozymes. Inducing an interaction between the loops on stems I and II is likely to stabilize this active conformation, consequently lowering the $Mg^{2+}$ concentration normally required to induce this change.

Very similar effects (an increase in catalytic activity combined with a reduced requirement for $Mg^{2+}$) were observed with the hairpin ribozyme after applying a topological change at the interdomain junction from a two- or three-way junction to the natural four-way junction[17–19]. Moreover, restricting the conformational flexibility of the minimalist HHRzs by chemically crosslinking helices I and II has been

shown to shift the HHRz internal equilibrium toward ligation[20,21]. A similar effect occurs with the hairpin ribozyme in the natural context of a four-way helical junction[22]. The involvement of the extra tertiary interacting elements in producing high catalytic activity at a low $Mg^{2+}$ concentrations[23,24] has been observed in large ribozymes such as group I introns[25], and may be a general characteristic of RNA structure and catalysis.

In summary, this study demonstrates that tertiary interactions between the nonessential and peripheral loops capping helices I and II are responsible for conferring the intracellular activity of natural hammerhead ribozymes, and are also required for artificial HHRz functionality in an intracellular environment. The topology of the junction in the hairpin ribozyme, and the loop-loop tertiary contacts in the hammerhead and large ribozymes, although nonessential and peripheral, seem to reduce the conformational space available to the structural elements, thereby promoting folding and the associated decrease in the requirement for divalent cations. Further structural and kinetic studies are needed to evaluate whether the conformational changes caused by these tertiary interactions induce additional conformational changes at the catalytic site capable of enhancing ribozyme activity.

## METHODS

**Transient reporter expression assay.** The transient reporter expression assay was based on an adeno-associated viral vector plasmid containing the SEAP gene cloned between the CMV promoter and BGH 3′ UTR. HHRzs were cloned into the *Xba*I and *Sal*I sites within the 3′ UTR. Recombinant plasmids (50 ng per well) were transfected into subconfluent HEK 293 cells grown in 96-well plates using Lipofectamin 2000 (Invitrogen). Protein level using the Great EscAPe SEAP assay kit (Clontech) and mRNA level using the branched-DNA assay[26] (Bayer) were quantified 24 h after transfection. For each HHRz construct, protein and mRNA levels were measured from three independent transfections; error bars indicate standard deviation from the average of triplicates.

**HHRzs sequence and synthesis.** HHRzs were synthesized by T7 transcription[27] in the presence of [α-$^{32}$P]UTP from synthetic DNA templates in the presence of 25- to 27-mer antisense DNA oligonucleotides complementary to the catalytic core. Full-length HHRzs were purified by PAGE under denaturing conditions. Cleavage rate was measured by incubating HHRzs in 50 mM Tris-HCl, pH 7.0, with indicated concentrations of $MgCl_2$ at 37 °C. Reactions were stopped by adding three volumes of 95% (v/v) formamide containing 30 mM EDTA. Cleavage products were resolved with 10% (w/v) PAGE under denaturing conditions and quantified by phosphoimager analysis. $k_{obs}$ values were calculated according to the equation $F_t = F_o + F_\infty(1 - e^{kt})$, as described[28].

The HH15 sequence was 5′-GGGAGCCCCGCUGAUGAGGUCGGGGA-GACCGAAAGGGACUUCGGUCCCUACGGGGCUCCC-3′. Three extra G-C base pairs were added to all ribozymes (sequences in **Fig. 2**) to ensure efficient *in vitro* transcription.

**Structural modeling.** All modeling and three-dimensional drawings were done using MANIP[14] and DRAWNA[29]. The coordinates for the modeled structure of the sTRSV ribozyme have been deposited in the Protein Data Bank (accession code 1P66).

ACKNOWLEDGMENTS

We thank O. Uhlenbeck, A. Wolfson, J. Rossi and D. Lilley for insightful discussions and critical reading of this manuscript, S. Suggs for comments and encouragement and A. Reynolds, M. Brewer and W. Marshall for their help and support.

COMPETING INTERESTS STATEMENT

The authors declare that they have no competing financial interests.

Received 11 March; accepted 8 July 2003
Published online at http://www.nature.com/naturestructuralbiology/

1. Ruffner, D.E., Stormo, G.D. & Uhlenbeck, O.C. Sequence requirements of the hammerhead RNA self-cleavage reaction. *Biochemistry* **29**, 10695–10702 (1990).
2. Darnell, J., Lodish, H.F. & Baltimore, D. *Molecular Cell Biology* (W.H. Freeman, New York, 1986).
3. Deshler, J.O., Li, H., Rossi, J.J. & Castanotto, D. Ribozymes expressed within the loop of a natural antisense RNA form functional transcription terminators. *Gene* **155**, 35–43 (1995).
4. Buzayan, J.M., Hampel, A. & Bruening, G. Nucleotide sequence and newly formed phosphodiester bond of spontaneously ligated satellite tobacco ringspot virus RNA. *Nucleic Acids Res.* **14**, 9729–9743 (1986).
5. Forster, A.C. & Symons, R.H. Self-cleavage of virusoid RNA is performed by the proposed 55-nucleotide active site. *Cell* **50**, 9–16 (1987).
6. Hernandez, C. & Flores, R. Plus and minus RNAs of peach latent mosaic viroid self-cleave *in vitro* via hammerhead structures. *Proc. Natl. Acad. Sci. USA* **89**, 3711–3715 (1992).
7. Long, D.M. & Uhlenbeck, O.C. Kinetic characterization of intramolecular and intermolecular hammerhead RNAs with stem II deletions. *Proc. Natl. Acad. Sci. USA* **91**, 6977–6981 (1994).
8. Long, D.M., LaRiviere, F.J. & Uhlenbeck, O.C. Divalent metal ions and the internal equilibrium of the hammerhead ribozyme. *Biochemistry* **34**, 14435–14440 (1995).
9. Pley, H.W., Flaherty, K.M. & McKay, D.B. Three-dimensional structure of a hammerhead ribozyme. *Nature* **372**, 68–74 (1994).
10. Scott, W.G., Finch, J.T. & Klug, A. The crystal structure of an all-RNA hammerhead ribozyme: a proposed mechanism for RNA catalytic cleavage. *Cell* **81**, 991–1002 (1995).
11. Hainzl, T., Huang, S. & Sauer-Eriksson, A.E. Structure of the SRP19 RNA complex and implications for signal recognition particle assembly. *Nature* **417**, 767–771 (2002).
12. Oubridge, C., Kuglstatter, A., Jovine, L. & Nagai, K. Crystal structure of SRP19 in complex with the S domain of SRP RNA and its implication for the assembly of the signal recognition particle. *Mol. Cell* **9**, 1251–1261 (2002).
13. Berman, H.M. *et al.* The nucleic acid database. A comprehensive relational database of three-dimensional structures of nucleic acids. *Biophys. J.* **63**, 751–759 (1992).
14. Massire, C. & Westhof, E. MANIP: an interactive tool for modelling RNA. *J. Mol. Graph. Mod.* **16**, 197–205 (1999).
15. McKay, D.B. Structure and function of the hammerhead ribozyme: an unfinished story. *RNA* **2**, 395–403 (1996).
16. Hammann, C., Norman, D.G. & Lilley, D.M. Dissection of the ion-induced folding of the hammerhead ribozyme using 19F NMR. *Proc. Natl. Acad. Sci. USA* **98**, 5503–5508 (2001).
17. Esteban, J.A., Banerjee, A.R. & Burke, J.M. Kinetic mechanism of the hairpin ribozyme. Identification and characterization of two nonexchangeable conformations. *J. Biol. Chem.* **272**, 13629–13639 (1997).
18. Zhao, Z.-Y. *et al.* The folding of the hairpin ribozyme: dependence on the loops and the junction. *RNA* **6**, 1833–1846 (2000).
19. Walter, N.G., Burke, J.M. & Millar, D.P. Stability of hairpin ribozyme tertiary structure is governed by the interdomain junction. *Nat. Struct. Biol.* **6**, 544–549 (1999).
20. Stage-Zimmermann, T.K. & Uhlenbeck, O.C. A covalent crosslink converts the hammerhead ribozyme from a ribonuclease to an RNA ligase. *Nat. Struct. Biol.* **8**, 863–867 (2001).
21. Blount, K.F. & Uhlenbeck, O.C. Internal equilibrium of the hammerhead ribozyme is altered by the length of certain covalent cross-links. *Biochemistry* **41**, 6834–6841 (2002).
22. Fedor, M.J. Tertiary structure stabilization promotes hairpin ribozyme ligation. *Biochemistry* **38**, 11040–11050 (1999).
23. Pan, J., Thirumalai, D. & Woodson, S.A. Magnesium-dependent folding of self-splicing RNA: exploring the link between cooperativity, thermodynamics, and kinetics. *Proc. Natl. Acad. Sci. USA* **96**, 6149–6154 (1999).
24. Pan, J. & Woodson, S.A. The effect of long-range loop-loop interactions on folding of the *Tetrahymena* self-splicing RNA. *J. Mol. Biol.* **294**, 955–965 (1999).
25. Lehnert, V., Jaeger, L., Michel, F. & Westhof, E. New loop-loop tertiary interactions in self-splicing introns of subgroup IC and ID: a complete 3D model of the *Tetrahymena thermophila* ribozyme. *Chem. Biol.* **3**, 993–1009 (1996).
26. Collins, M.L. *et al.* A branched DNA signal amplification assay for quantification of nucleic acid targets below 100 molecules/ml. *Nucleic Acids Res.* **25**, 2979–2984 (1997).
27. Milligan, J.F. & Uhlenbeck, O.C. Synthesis of small RNAs using T7 RNA polymerase. *Methods Enzymol.* **180**, 51–62 (1989).
28. Stage-Zimmermann, T.K. & Uhlenbeck, O.C. Hammerhead ribozyme kinetics. *RNA* **4**, 875–889 (1998).
29. Massire, C., Gaspin, C. & Westhof, E. DRAWNA: a program for drawing schematic views of nucleic acids. *J. Mol. Graph.* **12**, 201–206 (1994).
30. Hertel, K.J. *et al.* Numbering system for the hammerhead. *Nucleic Acids Res.* **20**, 12 (1992).
31. Gorodkin, J., Knudsen, B., Zwieb, C. & Samuelsson, T. SRPDB (Signal Recognition Particle Database). *Nucleic Acids Res.* **29**, 169–170 (2001).
32. Leontis, N.B. & Westhof, E. Geometric nomenclature and classification of RNA base pairs. *RNA* **7**, 499–512 (2001).

# Corrigendum: Sequence elements outside the hammerhead ribozyme catalytic core enable intracellular activity

**Anastasia Khvorova, Aurélie Lescoute, Eric Westhof & Sumedha D Jayasena**
*Nat. Struct. Biol.* **10,** 708–712 (2003).

Figure 4e in this paper contained mistakes. The labels for the fourth, fifth and sixth sets of data should be sTRSV + PL1, sTRSV + PL2 and sTRSV + PL1&2, respectively. We apologize for the inconvenience this may have caused.

# Erratum: Pulling geometry defines the mechanical resistance of a β-sheet protein

**David J Brockwell, Emanuele Paci, Rebecca C Zinober, Godfrey S Beddard, Peter D Olmsted, D Alastair Smith, Richard N Perham & Sheena E Radford**
*Nat. Struct. Biol.* **10,** 731–737 (2003).

A mistake was introduced during production of this paper. This mistake was on page 731, line 4 of the second paragraph in the 'Results' section. The correct sentence should read: "The parent $(I27)_5$ homopolymer has been described and is composed of five copies of a mutated C47S C63S domain[7,12]." We apologize for any inconvenience this may have caused.